

## Article

# Photobiomodulation Therapy Mitigates Salivary Gland Damage Induced by Radioactive Iodine Ablation

Luana Campos <sup>1,2,†</sup> , Gabriela Campos Magliano <sup>2,†</sup>, Andressa Matucci Hotsumi <sup>2</sup>, Daniele de Paula Faria <sup>3</sup>, Alexandre Teles Garcez <sup>3</sup>, Fernando Godoy <sup>4</sup>, Victor Elias Arana-Chavez <sup>2</sup>  and Alyne Simões <sup>2,\*</sup> 

- <sup>1</sup> Graduate Program in Implantology, School of Dentistry, University of Santo Amaro, São Paulo 04829-300, SP, Brazil; lucampos@prof.unisa.br
- <sup>2</sup> Laboratory of Oral Biology, Department of Biomaterials and Oral Biology, School of Dentistry, University of São Paulo, São Paulo 05508-000, SP, Brazil; gabrielacamposmagliano@gmail.com (G.C.M.); vearana@usp.br (V.E.A.-C.)
- <sup>3</sup> Department of Radiology and Oncology, School of Medicine (FMUSP), University of São Paulo, São Paulo 05403-010, SP, Brazil
- <sup>4</sup> Lemolab Clinical Analysis, São Paulo 02517-140, SP, Brazil
- \* Correspondence: lysimoes@usp.br; Tel.: +55-11-2648-8072
- † These authors contributed equally to this work.

**Abstract:** (1) Background: Thyroid tissue ablation with radioactive iodine (RAI) has been successfully used in the treatment of differentiated thyroid cancers. However, as a side effect, RAI may induce salivary gland (SG) hypofunction, which has been alternatively managed with photobiomodulation therapy (PBMT). In our study, we assessed the effects of RAI on the SGs and further analyzed whether PBMT can minimize tissue damage. (2) Methods: Balb/c mice were allocated into three groups, as follows: RI, submitted to RAI orally; RIL, similar to RI, but with PBMT for SG hypofunction; and C, control group. The animals were euthanized on days 0, 10, and 90 after RAI. (3) Results: A decrease in tri-iodothyronine (T3) and thyroxine (T4) serum levels was observed both in the RI and RIL groups. In addition, a decrease in SG weight and morphological alterations were shown in the RI group throughout the experimental period, as well as a significant increase in total protein and peroxidase concentrations, and catalase activity. On day 90, the RI group presented less collagen and fewer sodium/iodine channels, with higher rates of cell apoptosis. Perchnetate ( $\text{Na}^{99\text{m}}\text{TcO}_4$ ) uptake was also affected in the RI group in all experimental times. Interestingly, although the RIL group also presented some alterations regarding these parameters, they were not statistically different from those of the C group on day 90. (4) Conclusions: Our results provide evidence that RAI induces harmful effects on the SGs, which can be successfully managed with PBMT.

**Keywords:** thyroid neoplasms; iodine-131; xerostomia; low-level light therapy



**Citation:** Campos, L.; Magliano, G.C.; Hotsumi, A.M.; Faria, D.d.P.; Garcez, A.T.; Godoy, F.; Arana-Chavez, V.E.; Simões, A. Photobiomodulation Therapy Mitigates Salivary Gland Damage Induced by Radioactive Iodine Ablation. *Photonics* **2023**, *10*, 611. <https://doi.org/10.3390/photonics10060611>

Received: 25 March 2023

Revised: 18 May 2023

Accepted: 23 May 2023

Published: 25 May 2023



**Copyright:** © 2023 by the authors. Licensee MDPI, Basel, Switzerland. This article is an open access article distributed under the terms and conditions of the Creative Commons Attribution (CC BY) license (<https://creativecommons.org/licenses/by/4.0/>).

## 1. Introduction

Differentiated thyroid cancer (DTC) accounts for 90% of all thyroid cancers, with a substantial increase in the past three years. Over 50,000 new cases are estimated to be diagnosed in the United States by 2050 [1,2]. Generally, the most common therapeutic approach for DTC includes thyroidectomy followed by RAI ablation [3].

This approach consists of delivering iodine in thyroid cells through sodium iodide transporters and emitting beta (ionizing) radiation. RAI therapy has been used for the detection and removal of residual thyroid tissue and was proven beneficial in decreasing DTC recurrence [3,4]. However, albeit to a lesser degree, non-thyroidal tissues such as the lacrimal, nasopharynx, SGs, and the gastric and colonic mucosa, may accumulate iodine from the RAI ablation, which may result in adverse effects [5–7].

SGs are a group of exocrine glands that secrete saliva into the oral cavity and thereby play an important role in maintaining oral health, digestion, and speech. Among the

salivary constituents, catalase and peroxidase are two important antioxidant enzymes that protect cells and tissues from oxidative stress by catalyzing free radical reactions. Catalase converts  $H_2O_2$  into  $O_2$  and  $H_2O$ , whereas peroxidase catalyzes the conversion of thiocyanate into hypothiocyanate in the presence of  $H_2O_2$ , offering an antimicrobial and antioxidant function [8,9].

SGs are highly radiosensitive, and after being exposed to high doses of RAI, patients often develop pain and/or swelling, xerostomia, taste alterations, and an increased risk of oral diseases. Altogether, this may significantly impair the patient's long-term quality of life [7,10–12]. Curiously, RAI-induced SG hypofunction was first recognized 75 years ago but its pathobiology remains poorly understood until the present day. Some authors report that the adverse effects of RAI on the SGs probably start on striated ducts, which are responsible for expressing the sodium–iodine symporter (NIS) [10]. More than 20% of the administered iodine-131 ( $^{131}I$ ) dose is secreted into the salivary flow and, according to the literature, the inflammatory response of the patient generates ductal system constriction, resulting in saliva retention and symptoms of obstruction (sialadenitis) [7,10,13].

Currently, the management of SG hypofunction includes diverse palliative therapies, such as mouthwashes, salivary substitutes, parasympathomimetic drugs, acupuncture, and PBMT [14]. PBMT is a non-invasive and nonthermal therapy through which photons interact with the damaged tissue promoting analgesia, tissue regeneration, and modulation of inflammatory processes [15]. Using low-power lasers, PBMT has shown promising results for the prevention and management of SG hypofunction in non-cancer and cancer patients undergoing antineoplastic treatment [15–19].

Previous studies with RAI ablation have focused mostly on oral complaints and the clinical analysis of DTC patients, but little is known about the effects of this therapy on SGs. Thus, in our study, we assessed the effects of RAI on the SGs and further determined whether PBMT can mitigate tissue damage in a murine model, based on clinical, biochemical, morphological, and immunohistochemical analyses.

## 2. Materials and Methods

### 2.1. Animals

This study was previously approved by the Ethics Committee on Animal Use at the University of São Paulo School of Medicine (FMUSP, São Paulo, Brazil) (#017/16). Fifty-seven Balb/c male mice, aged 4 weeks, weighing approximately 20 g, were maintained under light and temperature-controlled conditions, with water and a standard diet ad libitum.

According to a previously published protocol for RAI-induced SG hypofunction in mice [15], the animals were randomly distributed into three groups, as follows: RI, submitted to RAI therapy; RIL, similar to the RI group, but with PBMT for the management of SG hypofunction; and C, a control group (untreated, RAI-free). In all experimental groups, RAI was administered orally (0.37 MBq/g body weight). The experimental period lasted 90 consecutive days and the animals were euthanized and analyzed at three different time points, as follows: day 0, before RAI ablation; day 10; and day 90 after RAI ablation.

Eight animals were euthanized at baseline, that is, before RAI ablation, to serve as a control group. The animals in the RI, RIL, and C groups were euthanized on day 10 ( $n = 10$ ,  $n = 10$ , and  $n = 8$  animals, respectively) and day 90 ( $n = 7$  animals per group) by administering 5% isoflurane in 100% oxygen before heart-stick euthanasia (Figure 1).

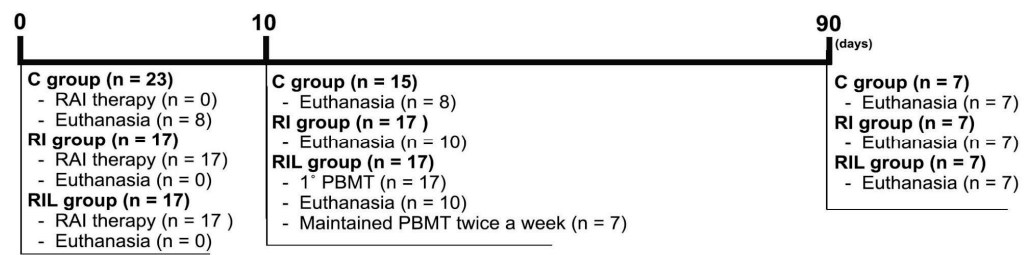


**Figure 1.** Study timeline showing the sequence of clinical procedures per group, over all experimental times. Experimental days are indicated in bold in the upper line, and the respective sample sizes are shown in parentheses.

## 2.2. PBMT Protocol

An InGaAlP diode laser (Therapy-DMC<sup>®</sup> Ltd.a, São Paulo, Brazil) set at 808 nm, 100 mW, 35 J/cm<sup>2</sup>, and 1 J of energy, delivered in 10 s per point was used (3 points per SG, bilaterally) in a perpendicular contact irradiation mode. This protocol was performed from day 10 to 90, twice a week.

## 2.3. Clinical Analysis

Full body and SG weight were measured in all experimental time points with the aid of a calibrated digital scale.

## 2.4. Tri-iodothyronine (T3) and Thyroxine (T4) Serum Levels

T3 and T4 concentrations were quantified in serum samples from all groups, collected from the heart immediately after euthanasia at all experimental time points. Serum T3 and T4 concentrations were measured in duplicate using a commercially available kit (T3 and T4. Interkit, Katal Biotecnológica Ind. Com. Ltd.a., Belo Horizonte, MG, Brazil).

## 2.5. Planar Scintigraphy Imaging

Animals in the RI and RIL groups were submitted to planar scintigraphy imaging (Triumph Trimodality, Gamma Medica Ideas, Los Angeles, CA, USA) throughout the experimental period (days 0, 10, and 90). Pertechnetate (Na<sup>99m</sup>TcO<sub>4</sub>, 33 MBq in 0.1 mL) was administered into the penile vein of anesthetized mice (isoflurane 3 vol.% in 100% O<sub>2</sub>). The animals were kept unconscious during the entire imaging protocol.

Dynamic planar scintigraphy images were acquired for 25 min (30 s per image), starting 5 min after Na<sup>99m</sup>TcO<sub>4</sub> injection, using a dual-head camera with 1.0 mm pinhole collimators and cadmium zinc telluride detectors. To stimulate the SGs, three drops of lemon were administered intraorally after planar scintigraphy had been in progress for 15 min.

## 2.6. Biochemical Analysis

The parotid (P) and submandibular (SM) glands were immediately removed, weighed, and stored in a freezer at −80 °C. Then, SG specimens were thawed, homogenized, and centrifuged following enzymatic assays.

The total protein concentration was determined by the Lowry method using the Folin-phenol reagent and bovine serum albumin as a standard. The plates were read at 660 nm in a Beckman DU-68 spectrophotometer [20]. Peroxidase concentration was measured at 460 nm following Chandra's method [21] modified by Anderson [22], with the samples diluted in phosphate buffer and 1 mM o-dianisidine. Catalase activity was measured at 240 nm by the Aebi method [23]. The catalysis of H<sub>2</sub>O<sub>2</sub> was observed by a decrease in absorbance per unit of time.

## 2.7. Histological Analysis

### 2.7.1. Morphological Analysis and the TUNEL Assay

Immediately after euthanasia, P and SM specimens from three animals per group, in each experimental time point, were fixed in 4% formaldehyde and 0.1% glutaraldehyde buffered in 0.1 M sodium cacodylate (pH 7.2) for 6 h at room temperature. For light microscopy, the samples were processed and included in paraffin. Three- $\mu\text{m}$ -thick sections were obtained in a MICROM HM360 microtome. Samples were stained with hematoxylin and eosin, examined, and photographed in an Olympus BX 60 light microscope.

Cell apoptosis in SG tissues was quantified by the TUNEL assay using ApopTag Plus Peroxidase (In Situ Apoptosis Kit, Millipore, Burlington, MA, USA) on days 10 and 90 following RAI therapy. TUNEL-positive cells were detected in 4- $\mu\text{m}$ -thick sections at 400 $\times$  magnification. The number of apoptotic cells was counted in three random fields per tissue section, according to the manufacturer's recommendations [24].

### 2.7.2. Mallory's Trichrome Deconvolution

Three- $\mu\text{m}$ -thick sections were obtained in a MICROM HM360 microtome. Specimens were stained using Mallory's Trichrome technique, followed by fuchsin, aniline blue, and orange G staining, according to the manufacturer's recommendations [25].

## 2.8. Immunohistochemical Analysis-NIS

NIS expression was determined using a sodium-iodine symporter polyclonal antibody (Proteintech, 24324-1 AP, San Diego, CA, USA) in 4- $\mu\text{m}$ -thick sections on a silanized slide. After deparaffinization, specimens were incubated in 3% hydrogen peroxide, followed by the addition of the primary antibody (sodium-iodine symporter polyclonal antibody G-5) diluted 1:500 for 60 min at room temperature. Then, the secondary antibody Histofine, Nichieri Biosciences Inc. (Rat MAX PO-MULTI-Universal Immuno-peroxidase Polymer for rat tissue, Anti-mouse and Rabbit, Chuo-ku, Tokyo) was added for 20 min. Sections were counterstained with Harris hematoxylin. A negative control was included by blocking the primary antibody [26].

## 2.9. Statistical Analysis

Data were analyzed by Student's *t*-test and two-way analysis of variance (ANOVA) with Tukey's post-hoc test. Differences were considered statistically significant at  $p < 0.05$ .

## 3. Results

### 3.1. Full Body and SG Weight

A significant increase in body weight was observed in all groups after 3 months as compared to baseline (day 0) (Figure 2A). In particular, the weight of the P glands in the RI group was reduced when compared to RIL and C groups after 90 days post-RAI therapy ( $p < 0.05$ ) (Figure 2B). The weight of the SM glands in the RI group was significantly reduced on days 10 and 90 when compared to the C group ( $p = 0.0053$  and  $p = 0.0254$ , respectively) (Figure 2C).

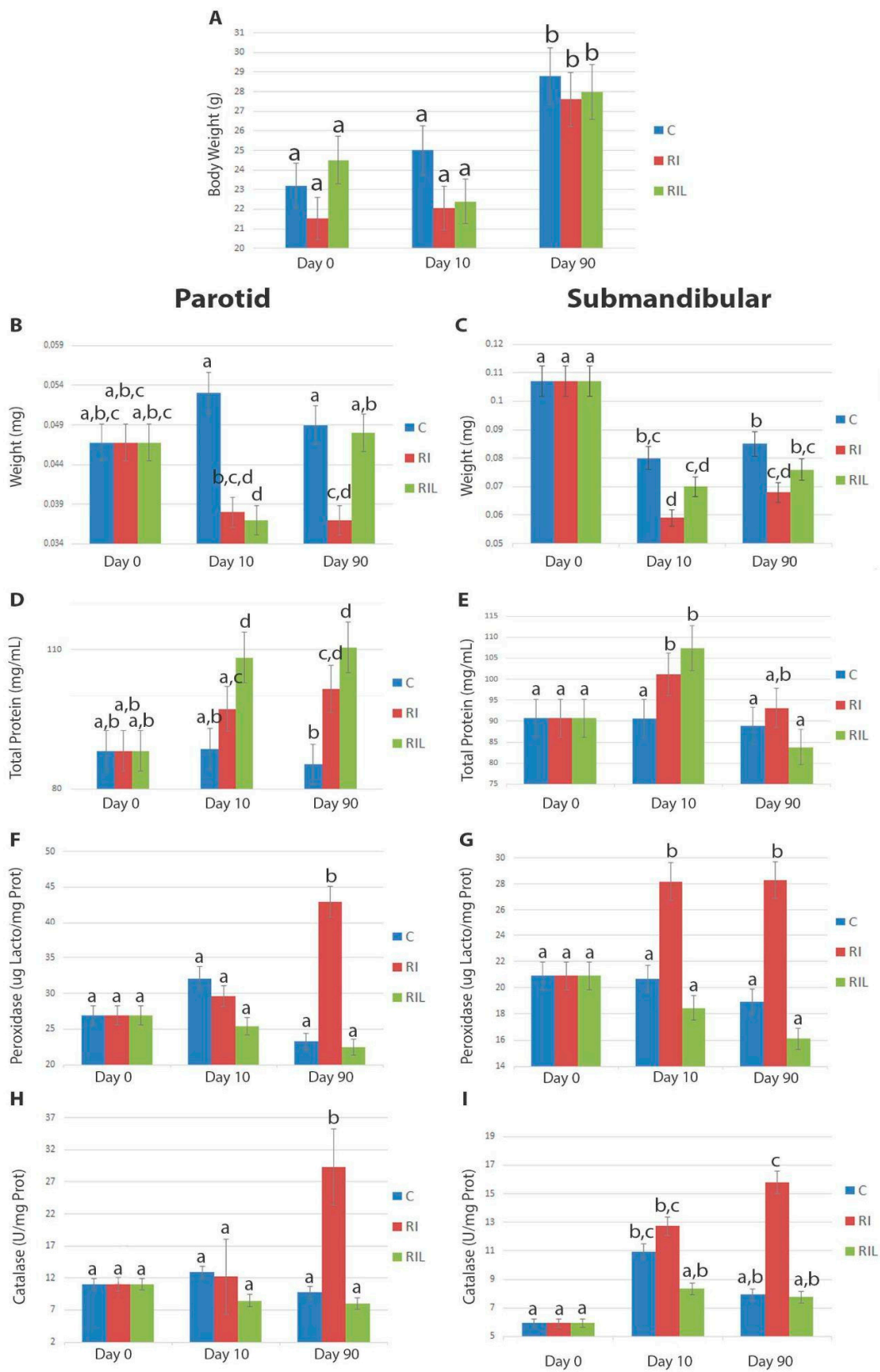


**Figure 2.** Clinical and biochemical data. (A) Comparison of full body weight. (B,C) Comparison of SG weight-P and SM, respectively. (D,E) Total protein concentration of the P and SM glands, respectively. (F,G) Peroxidase concentration of the P and SM glands, respectively. (H,I) Catalase activity of the P and SM, respectively. Different letters indicate statistically significant differences ( $p < 0.05$ ).

### 3.2. Biochemical Changes

A significant increase in the total protein concentration was observed in the P gland in the RI group on day 90. A significant increase in the peroxidase concentration and catalase activity was observed both in the P and SM glands in the RI group after three months compared to baseline and the C group (Figure 2D–I).

The P gland of RIL animals showed greater total protein concentration on day 10, which remained as so on day 90 when compared to the C group ( $p < 0.0001$ ). In contrast, the P gland of RI animals showed an increase in total protein concentration only on day 90 ( $p < 0.0013$ ) (Figure 2D). Moreover, only the RI group showed a significant increase in peroxidase concentration and catalase activity after 90 days, while the RIL group remained with values similar to those of the C group. The increase in peroxidase concentration on day 90 among RI animals was approximately 80% when compared to the other groups ( $p = 0.0001$ ). Likewise, catalase activity was greater in the RI group on day 90 ( $p = 0.001$ ) (Figure 2F,H).

The total protein concentration of SM specimens from the RI and RIL groups increased by ~10 and 15%, respectively in 10 days ( $p < 0.05$ ) and returned to baseline levels after 90 days. In contrast, peroxidase concentration was higher only in the RI group on days 10 and 90 ( $p = 0.009$  and  $p = 0.008$ ) (Figure 2G). The same occurred for catalase activity, where a significant increase was observed on day 90, when compared to day 0 ( $p = 0.0002$ ) and the control group ( $p = 0.0021$ ). The RIL group showed peroxidase concentration and catalase activity similar to that of the C group overall experimental times (Figure 2I).

### 3.3. Serum Measurements

Serum T3 and T4 concentrations dropped in all RAI-treated mice (RI and RIL groups) compared to untreated animals ( $p < 0.0001$ ) on day 10 and remained until day 90. These findings corroborate the effects of RAI in this study model (Figure 3).

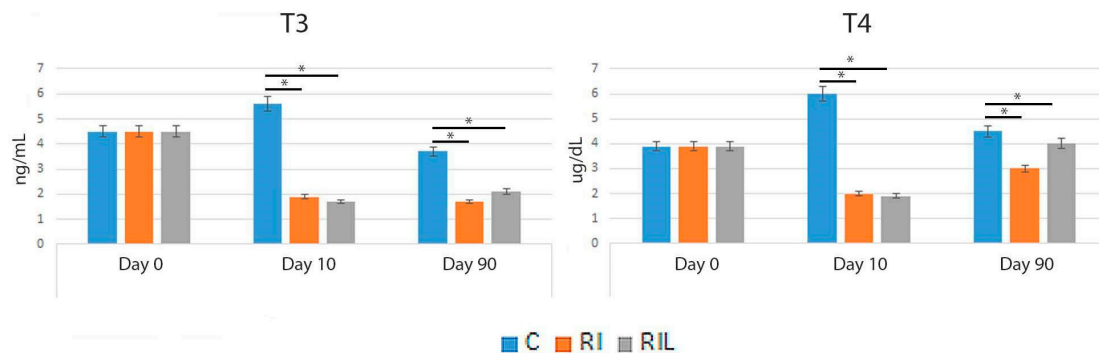


**Figure 3.** Serum T3 and T4 concentrations in RAI-treated mice. Asterisks (\*) indicate statistically significant differences ( $p < 0.05$ ).

### 3.4. Planar Scintigraphy Imaging

Scintigraphy imaging data of the P and SM glands from all RAI-treated animals (day 10) were computed similarly, as these analyses were performed shortly before the start of PBMT and, therefore, the RI and RIL groups still presented the same clinical condition. The P gland had a 15% decrease in  $\text{Na}^{99\text{m}}\text{TcO}_4$  uptake 10 days after RAI ablation ( $p < 0.0001$ ). After 90 days, the RI group maintained a decrease in  $\text{Na}^{99\text{m}}\text{TcO}_4$  uptake ( $p < 0.01$ ), while the RIL group returned to baseline levels (day 0) (Figure 4).

Similarly,  $\text{Na}^{99\text{m}}\text{TcO}_4$  uptake in the SM gland also decreased 10 days after RAI ablation ( $p < 0.0001$ ). After 90 days, the RI group showed  $\text{Na}^{99\text{m}}\text{TcO}_4$  uptake levels higher than those of other groups at the last time points, even though the average between the groups was similar (Figure 4).

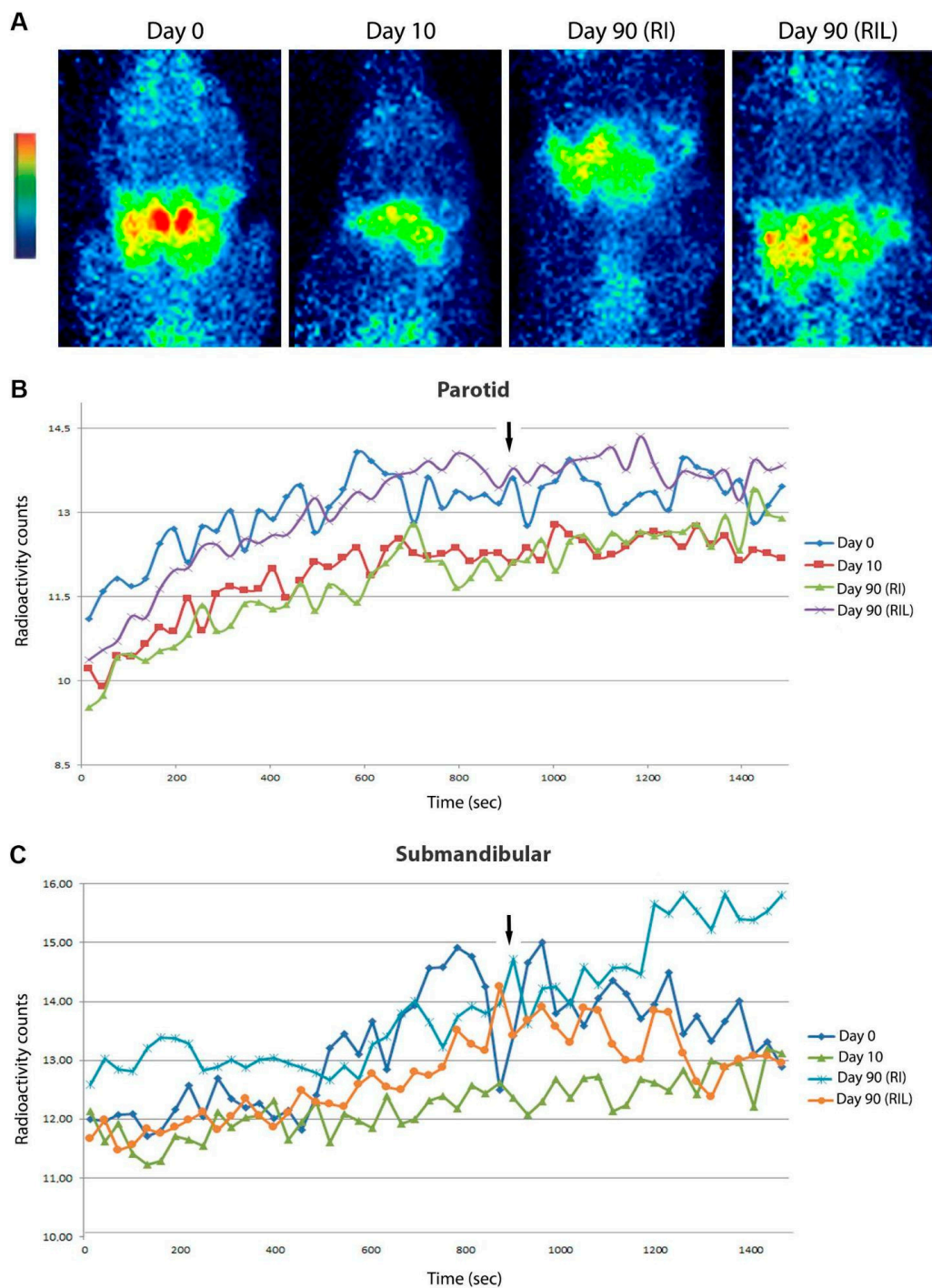


**Figure 4.** (A) Neck transaxial planar scintigraphy images at three different experimental time points. (B) Dynamics of  $\text{Na}^{99\text{m}}\text{TcO}_4$  radioactivity uptake in the P and (C) SM glands at baseline, T1, and T2. The arrows indicate the time of lemon administration. The x-axis denotes time (seconds), and the y-axis refers to radioactivity counts.

### 3.5. Histological Changes

#### 3.5.1. Cell Morphology and Apoptosis

For P glands, 10 days after RAI ablation, light microscopy images are suggestive of early acinar atrophy with an increase in intercellular space (Figure 5C). After 90 days, the morphological aspect of the RI group shows terminal secretory unit cells exhibiting mostly pale cytoplasm, as well as inflammatory infiltrate cells (Figure 5E). In contrast, the morphological aspect of the RIL group shows the recovery of glandular tissue and the

absence of inflammatory cells (Figure 5G). As for SM glands, no morphological changes were found throughout the experimental period (Figure 5B,D,F,H).

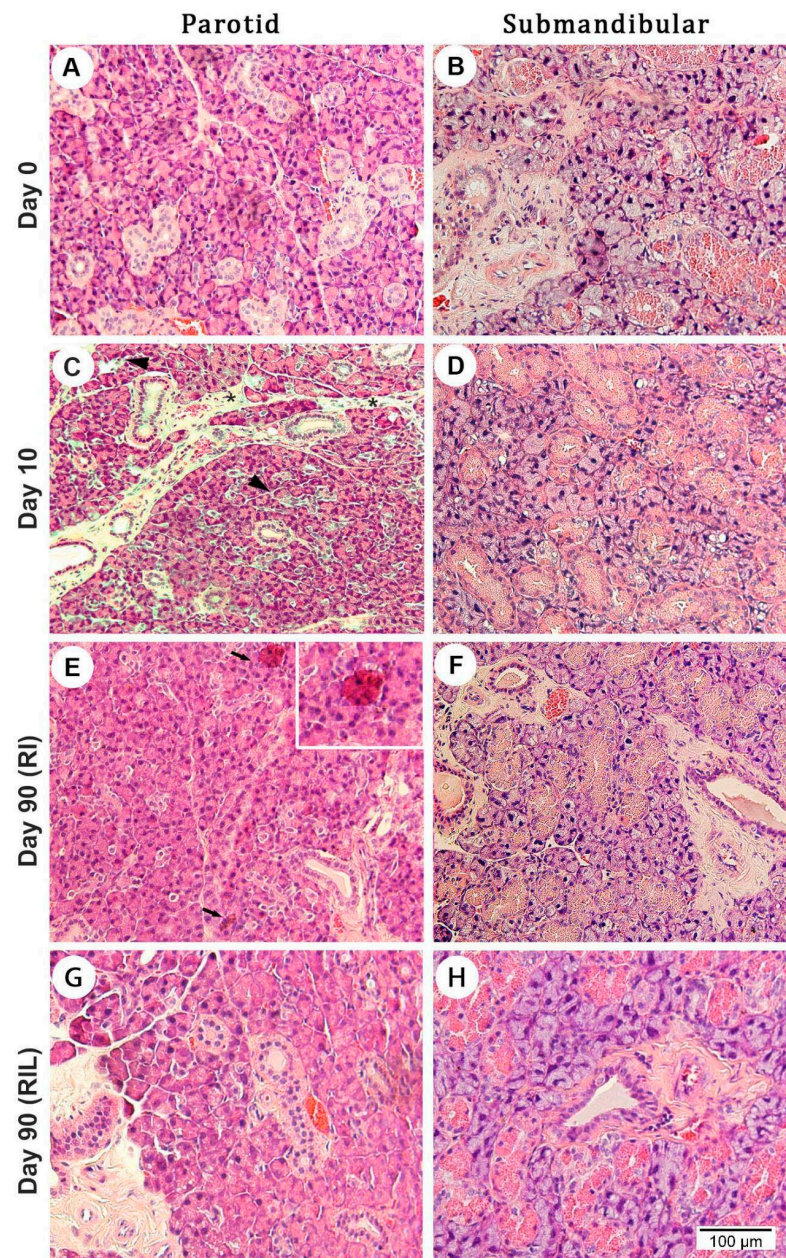


**Figure 5.** Light micrographs of the P glands (A,C,E,G) and SM glands (B,D,F,H) of RAI-treated mice. In (A), the P gland shows a normal structure, with healthy terminal secretory units and ducts. (C) shows early acinar atrophy with an increase of intercellular space (triangle) and enlargement of connective tissue septum (\*) in the RI and RIL groups. In (E), the morphological aspect of the RI group shows terminal secretory unit cells exhibiting mostly pale cytoplasm, as well as inflammatory infiltrate cells (arrows). In (G), the morphological aspect of the RIL group shows the recovery of glandular tissue and the absence of inflammatory cells. In (B), the SM gland shows normal terminal secretory units and ducts, which was further observed at the other experimental time points [days 10 (D) and 90] in both RI (F) and RIL (H) groups. Original magnification: 20 $\times$ , hematoxylin and eosin staining-Bar with 100  $\mu$ m.

The TUNEL assay for cell apoptosis showed that the control group for both glands and experimental time points exhibited approximately one apoptotic cell per field. RAI-treated groups (RI and RIL) showed a range of 30–45 apoptotic cells on day 10, for both glands, with a significant difference compared to the control ( $p < 0.05$ ). On day 90, a greater number

of apoptotic cells ( $n = 25/\text{field}$ ) was observed in P specimens from the RI group compared to the control ( $n = 1/\text{field}$ ) ( $p < 0.05$ ). The RIL group showed apoptotic cell counts similar to those of the control group ( $p > 0.05$ ). As for SM specimens, no difference was found between the groups, with fewer than 5 apoptotic cells per field on day 90 (Figure 6).

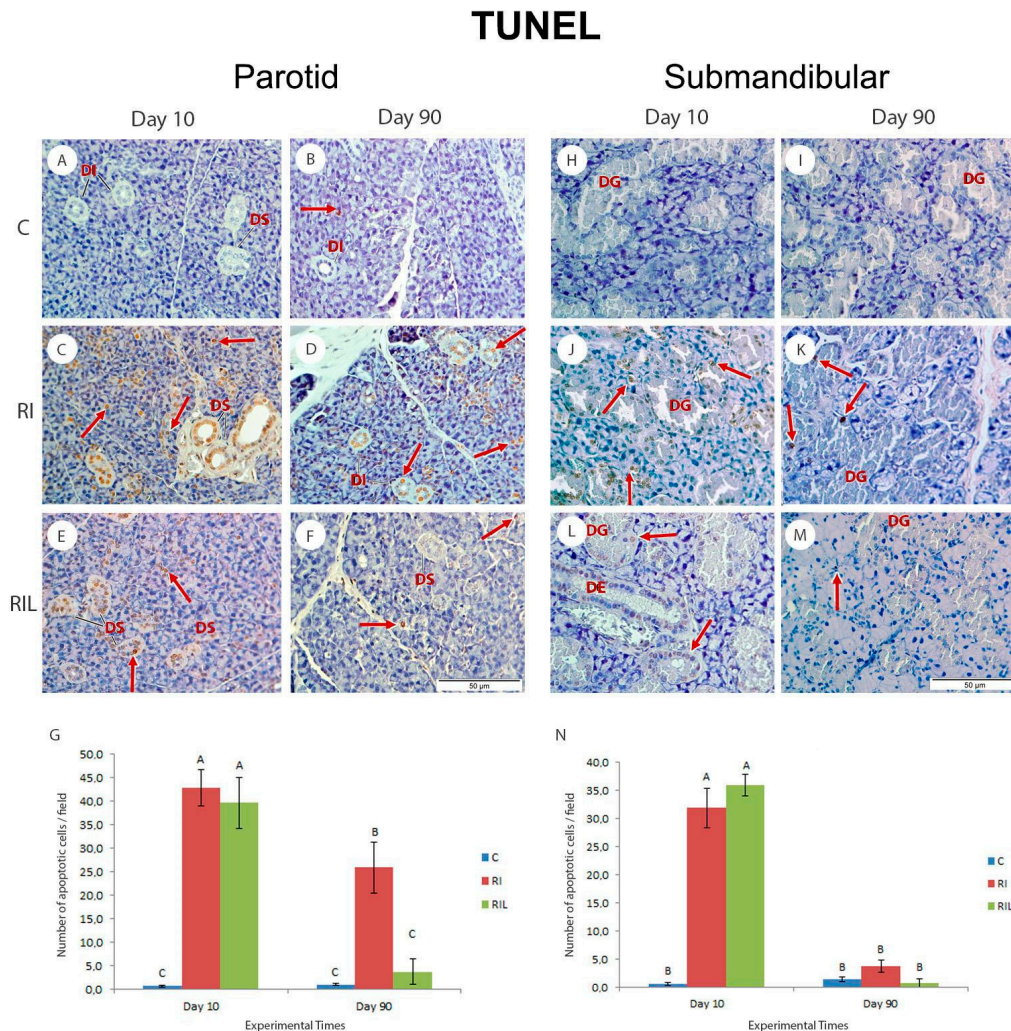


**Figure 6.** TUNEL immunohistochemical photomicrographs and analysis of the number of apoptotic cells expressed in the P and SM glands on days 10 and 90. For P glands, in (A,B), the C group on day 10, showed the absence of labeling, and on day 90 revealed an apoptotic nucleus (arrow) in the secretory unit. In (C,E), the RI and RIL groups on day 10 showed multiple apoptotic nuclei in the secretory unit and ducts. In (D), the RI group on day 90, shows the permanence of labeling in acinar cells and ducts. In (F), the RIL group was on day 90, with less intense labeling. For SM glands, in (H,I), the control group on days 10 and 90, showed the absence of labeling. In (J,L), the RI and RIL groups on day 10 showed apoptotic nuclei in the secretory unit and ducts (arrows). In (K,M), both RI and RIL groups on day 90, showed less markup (arrows). In (G,N), the number of apoptotic cells for P and SM glands, respectively, on days 10 and 90. Different letters represent statistical differences ( $p < 0.05$ ). DG Granular Duct, ID, Intercalary Duct; DS, Striated Duct; ED, Excretory Duct; VS, Vase Sanguine. Original Magnification:  $40\times$  -Staining: Hematoxylin-Bar with  $50\ \mu\text{m}$ .

### 3.5.2. Mallory’s Trichrome

Mallory’s Trichrome staining was used to determine the concentration of collagen (blue-colored) in the SM and P glands of animals. Photomicrographs of the P gland on day 10 showed a collagen concentration of 15%, 5.5% and 7.5% in the control, RI and RIL groups, respectively ( $p < 0.05$ ). After 90 days, the group submitted to PBMT showed a % collagen concentration

equal to the control (15%). On the other hand, parotid specimens from the RI group showed a collagen concentration of 8%, with no significant difference from the control ( $p > 0.05$ ) (Figure 7). Similarly, photomicrographs of SM specimens on day 10 showed a collagen concentration of approximately 5% in RAI-treated groups as compared to 19% in the C group ( $p < 0.05$ ). After 90 days, only the RI group showed a decrease in collagen concentration (6.8%) compared to the control (13%), which was statistically significant ( $p < 0.05$ ) (Figure 7).

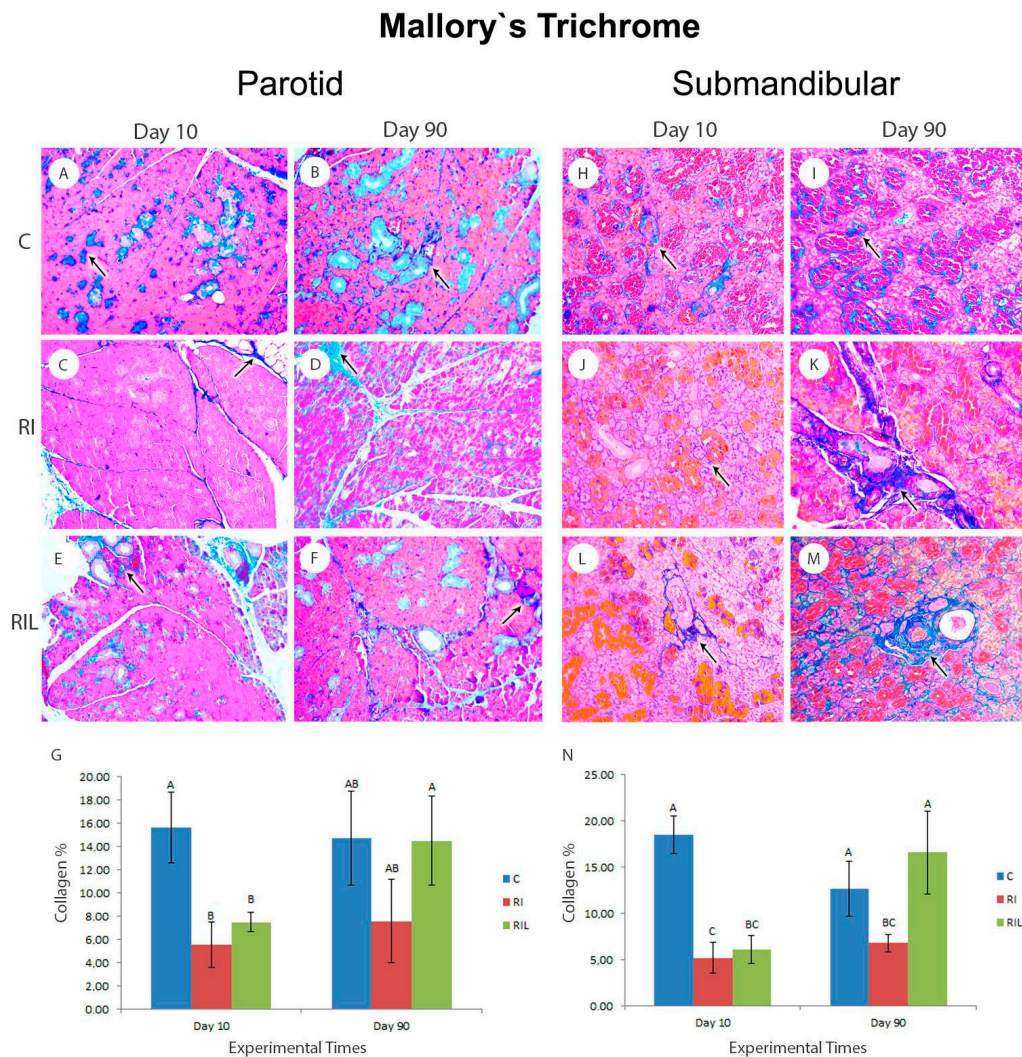


**Figure 7.** Photomicrograph of SGs, stained with Mallory's Trichrome (arrows), and deconvolution, for determination of collagen concentration. For the P glands, in (A,B), the C group on days 10 and 90, revealed normal collagen staining. In (C,E), the RI and RIL groups on day 10, showed less collagen staining when compared with the control group. In (D), a slight increase in collagen staining for the RI group on day 90. In (F), a considerable increase in collagen staining for the RIL group on day 90. For SM glands, in (H,I) the C group on days 10 and 90, also revealed normal collagen staining. In (J,L), the RI and RIL groups on day 10, showed less collagen staining when compared with the control group. In (K,M), the RI and RIL groups on day 90, a greater presence of collagen is observed, indicating a possible region of fibrosis (arrow). In (G,N), Mallory's Trichrome deconvolution for P and SM glands, respectively, show the averages of the percentage amounts of collagen on days 10 and 90. Different letters represent statistical differences ( $p < 0.05$ ). Original magnification  $20\times$  -Bar with  $100\ \mu\text{m}$ .

### 3.5.3. Immunohistochemical Analysis-NIS

An immunohistochemical assay was performed to measure NIS expression in P and SM specimens at different experimental time points. NIS protein was present mainly in striated ducts,

and in some cases, in intercalated ducts. The photomicrographs of both SGs showed reduced NIS staining in RAI-treated groups (RI and RIL) on day 10, when compared to the control group ( $p < 0.05$ ). In contrast, on day 90, NIS staining levels in the laser-treated group were similar to those of the control, for both SGs, which was not observed in the RI group (Figure 8).

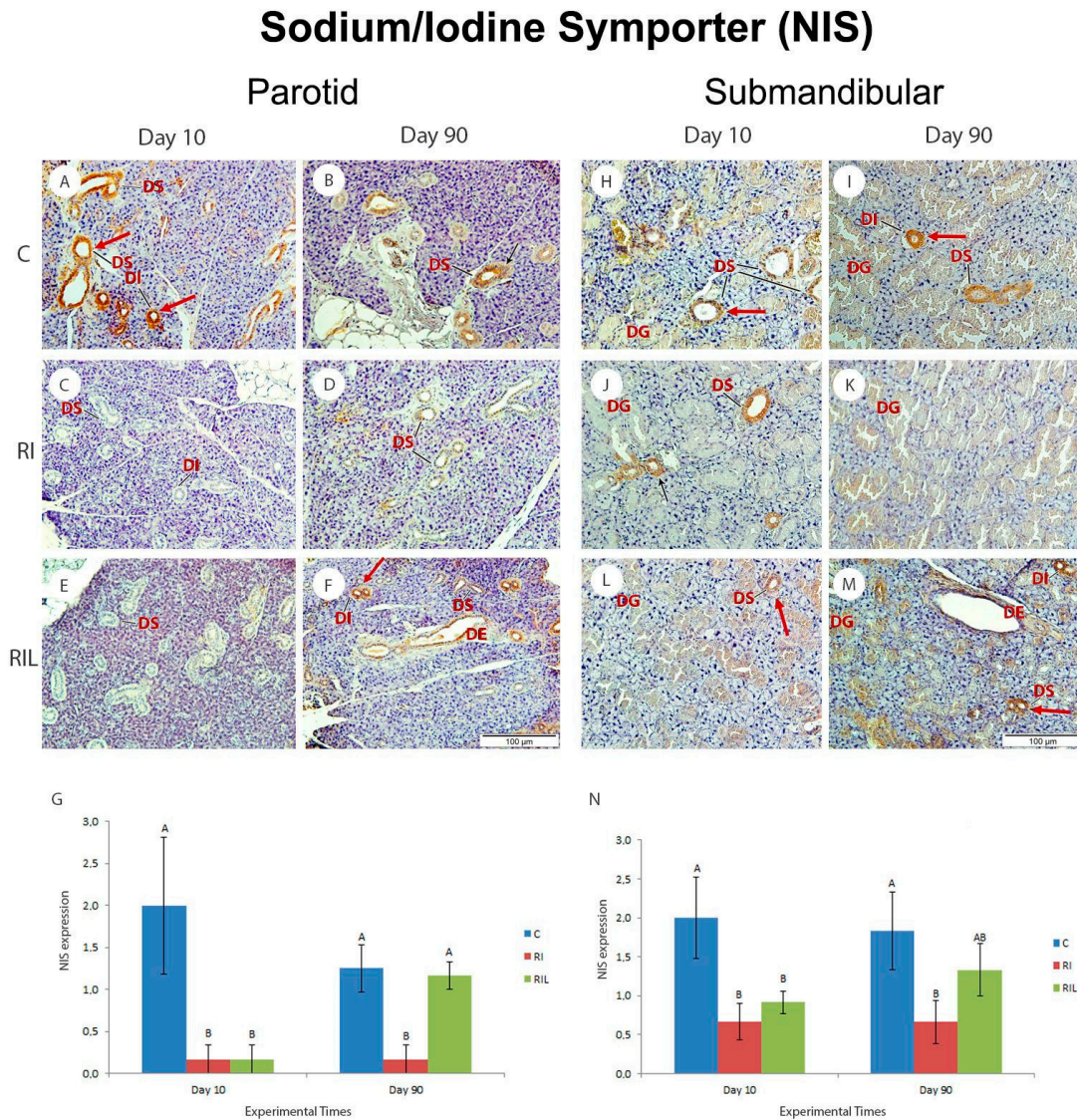


**Figure 8.** Photomicrograph and graphs of quantification of SGs in the immunohistochemical analysis of NIS, for detection of sodium and iodine channel expression. For P glands, in (A,B), the C group on days 10 and 90, respectively, labeling of NIS in the intercalated and striated (arrow). In (C,E), RI and RIL groups on day 10, it is possible to observe the absence of labeling in the ducts. In (D), the RI group on day 90, it is notable that the absence of NIS labeling in the ducts has been maintained. In (F), the RIL group on day 90, NIS labeling is observed in the intercalated and striated ducts. For SM glands, in (H,I), the C group on days 10 and 90, respectively, labeling of NIS in the intercalated and striated ducts (arrow). In (J,L), the RI and RIL groups on day 10, showed evident labeling of NIS in the intercalated and striated ducts (arrows). In (K), the RI group on day 90, showed the absence of NIS labeling in the ducts. In (M), the RIL group on day 90, the NIS labeling is observed in the intercalated and striated ducts (arrows). In (G,N), the quantification of NIS labeling for P and SM glands, respectively, on days 10 and 90, was expressed. Equal letters indicate similarity and different letters indicate statistically significant differences between each group at different experimental times or between groups at the same experimental time. ID, intercalary duct; DS, Striated Duct; ED, Excretory Duct; SV, Blood Vessel. Original Magnification: 20× -Staining: Hematoxylin-Bar with 100 μm.

#### 4. Discussion

In recent years, the use of RAI after thyroidectomy has been increasing in patients with DTC. Yet, the administration of high doses of iodine can result in necrosis of follicular cells [27]. This type of radioisotope is given orally and generates intense thyroiditis (inflammation), resulting in the inability of the thyroid to synthesize its hormones, as observed in our study. The side effects of RAI therapy on healthy tissues remain uncertain and conflicting [1,2], hence it is essential to better understand and minimize them. Although little is known about the effects of RAI on the clinical and morphological aspects of SGs [10], xerostomia/hypofunction of the SG has been seen as a side effect in patients who undergo antineoplastic treatment with iodotherapy. This may significantly impact the quality of life of cancer patients in addition to being an important factor to consider since these patients have a high survival rate [10,26,28–31].

Consistent with preliminary literature data, our findings showed that RAI therapy affects the function and morphology of SGs in mice, specifically by inhibiting NIS expression, increasing cell apoptosis, altering the glandular stroma, decreasing the collagen content, and atrophying secretory units in the SGs. In addition, our data pointed to an increase in the total protein and peroxidase concentrations, and catalase activity as well as changes in  $\text{Na}^{99\text{m}}\text{TcO}_4$  uptake. PBMT was effective in modulating the effects of this inflammatory condition by increasing collagen production in the glandular tissue, decreasing antioxidant enzymatic activity, reactivating NIS expression, and controlling cell apoptosis [32–34]. In general, the RIL group showed values similar to the control group.

Choi et al., (2013) showed no significant difference in mice body mass after 90 days of RAI ablation, which is in agreement with our findings. However, these authors found a decrease in SG weight in treated versus untreated animals [25], possibly indicating progressive acinar atrophy, which could in part justify the sialadenitis symptoms reported by patients undergoing RAI therapy. Atrophy of terminal secretory cells and the inflammatory cell infiltrate are classic histological signs of sialadenitis [4,13,35].

Apoptosis is a programmed cell death process that can occur in pathological conditions and, when it happens in large volume, may lead to the involution of an organ. This could explain the SG damage after RAI protocol, according to Choi et al., (2013) [25]. In agreement with that, the TUNEL assay data from RAI-treated groups revealed a higher amount of apoptotic cells, both in terminal secretory units and ducts, on day 10 of the experiment.

The amount of collagen in both P and SM glands was significantly reduced in RAI-treated groups on day 10. This may be related to the inflammatory process that occurs during the first few days after treatment with  $^{131}\text{I}$ , since collagen degradation begins early and is very active during the inflammatory process [4,25]. However, after 90 days, the RIL group showed a percentage collagen concentration equal to the control, unlike the group without laser (RI). Thus, our data suggest that the RIL group went through the SG inflammation phase more quickly, entering a process of tissue remodeling more quickly and effectively than the untreated group.

The concentration of RAI is known to be 20–100 times higher in saliva than in plasma [7,10]. This suggests that iodine, whether in its radioactive form or not, is absorbed and eliminated in large quantities by the SGs. The complete mechanism(s) by which this occurs is not yet fully understood, but one of the most widely accepted hypotheses is that there is an NIS in the striated ducts of the SGs, which is the transporter protein responsible for the entry of iodine into the SGs [36]. Our immunohistochemical analysis revealed the presence of NIS in the SGs of control animals, mainly in the striated ducts, as described in the literature [36].

In our study, while the striated ducts were strongly stained for NIS in the control group, they were not stained in RAI-treated groups on day 10. This is probably due to the thyroid's ability to decrease or block its functions in the face of high concentrations of iodine, which in some cases can be toxic [7,37]. Remarkably, when the SGs were submitted to PBMT, NIS expression returned to control-like values for both SGs.

Previous studies indicated that the biological damage caused by RAI therapy originates from a primary physical interaction through which radiation causes the excitation or ionization

of cells, breaking the chemical bonds and generating free radicals. This could explain the remarkable increase in the concentration and activity of peroxidase and catalase enzymes, respectively, for both SGs in the RI group. If the excess free-radical generation is not controlled, direct damage to cell components (proteins, DNA, etc) may occur [37,38]. The RIL group (submitted to RAI and PBMT) showed peroxidase concentration and catalase activity similar to the control group. Taken altogether, PBMT seems to mitigate RAI-induced SG damage.

Scintigraphy imaging is a well-established technique for the assessment of SG function as it reveals the spatial distribution of  $\text{Na}^{99\text{m}}\text{TcO}_4$  uptake and excretion in the SGs. Abnormal SG scintigraphic findings in patients submitted to RAI therapy vary considerably (37–72%) [16,31,39,40]. In our study, scintigraphy data showed a decrease in  $\text{Na}^{99\text{m}}\text{TcO}_4$  uptake in RAI-treated mice, which was more intense in the P glands. These results are in agreement with the literature [41] and the TUNEL data, showing that the P glands were more radiosensitive than the SM glands since the former are composed almost entirely of serous cells [42]. Despite the attempt of glandular stimulation, the administration of lemon was not able to alter  $\text{Na}^{99\text{m}}\text{TcO}_4$  excretion, probably due to swallowing alterations and a reduction in the lemon stimulation induced by the anesthetic agent [43].

## 5. Conclusions

Our murine study model suggests that RAI therapy can induce alterations in the structure and function of P and SM glands and that PBMT may be a promising alternative for the management of this complication. Moreover, our study provides evidence to support further research on the effects of RAI on the SGs and its mechanism(s) of action as well as dosimetric aspects related to PBMT.

**Author Contributions:** L.C., G.C.M., D.d.P.F. and A.S. conceived the idea and designed the experiments. L.C., G.C.M., A.M.H., D.d.P.F., A.T.G. and F.G. led the experiments. L.C., G.C.M., V.E.A.-C. and A.S. contributed to data analysis. L.C., G.C.M. and A.S. wrote the paper. All authors have read and agreed to the published version of the manuscript.

**Funding:** This study was financed in part by the Coordenação de Aperfeiçoamento de Pessoal de Nível Superior-Brasil (CAPES)—Finance code 001, related to G.C.M.'s master's scholarship and L.C.'s postdoctoral scholarship. In addition, this study was partially supported by the Fundação Faculdade de Odontologia (FFO-FUNDECTO).

**Institutional Review Board Statement:** Not applicable.

**Informed Consent Statement:** Not applicable.

**Data Availability Statement:** Not applicable.

**Acknowledgments:** CAPES and FUNDECTO for financial support.

**Conflicts of Interest:** The authors declare no conflict of interest.

## List of Abbreviations

Abbreviation	Nomenclature
RAI	Radioactive iodine
SG	Salivary gland
T3	Tri-iodothyronine
T4	Thyroxine
PBMT	Photobiomodulation therapy
DCT	Differentiated thyroid cancer
NIS	Sodium–iodine symporter
$^{131}\text{I}$	Iodine-131
FMUSP	University of São Paulo School of Medicine
P	Parotid
SM	Submandibular

## References

1. Nguyen, Q.T.; Lee, E.J.; Melinda, G.H.; Huang, G.; Young, I.P.; Park, I.; Khullar, A.; Plodkowski, R.A. Diagnosis and Treatment of Patients with Thyroid Cancer. *Am. Hea. Drug Benef.* **2015**, *8*, 30–40.
2. Haddad, R.I.; Bischoff, L.; Ball, D.; Bernet, V.; Blomain, E.; Busaidy, N.L.; Campbell, M.; Dickson, P.; Duh, Q.Y.; Ehya, H.; et al. Thyroid Carcinoma, Version 2.2022, NCCN Clinical Practice Guidelines in Oncology. *JNCCN J. Natl. Compr. Cancer Netw.* **2022**, *20*, 925–951. [[CrossRef](#)] [[PubMed](#)]
3. Sawka, A.M.; Thephamongkhol, K.; Brouwers, M.; Thabane, L.; Browman, G.; Gerstein, H.C. A Systematic Review and Meta-analysis of the Effectiveness of Radioactive Iodine Remnant Ablation for Well-Differentiated Thyroid Cancer. *J. Clin. Endocrinol. Metab.* **2004**, *89*, 3668–3676. [[CrossRef](#)] [[PubMed](#)]
4. Van Nostrand, D. Sialoadenitis Secondary to 131I Therapy for Well-Differentiated Thyroid Cancer. *Oral. Dis.* **2011**, *17*, 154–161. [[CrossRef](#)]
5. Barrueco, A.S.; Galán, F.G.; Rueda, I.A.; Coello, J.M.S.; Dorado, M.P.B.; Aubá, J.M.V.; Escanciano, M.E.; Jiménez, L.L.; Fernández, I.M.; Español, C.C. Incidence and Risk Factors for Radioactive Iodine-Induced Sialadenitis. *Acta Otolaryngol.* **2020**, *140*, 959–962. [[CrossRef](#)]
6. Choi, J.-S.; Hong, S.B.; Hyun, I.Y.; Lim, J.-Y.; Kim, Y.-M. Effects of Salivary Secretion Stimulation on the Treatment of Chronic Radioactive Iodine-Induced Sialadenitis. *Thyroid* **2015**, *25*, 839–845. [[CrossRef](#)]
7. Mandel, S.J.; Mandel, L. Review Radioactive Iodine and the Salivary Glands. *Thyroid* **2003**, *13*, 265–271. [[CrossRef](#)]
8. Ibuki, F.K.; Simões, A.; Nicolau, J.; Nogueira, F.N. Laser Irradiation Affects Enzymatic Antioxidant System of Streptozotocin-Induced Diabetic Rats. *Lasers Med. Sci.* **2013**, *28*, 911–918. [[CrossRef](#)]
9. Campos, L.; Nicolau, J.; Arana-Chavez, V.E.; Sim, A. Effect of Laser Phototherapy on Enzymatic Activity of Salivary Glands of Hamsters Treated with 5-Fluorouracil. *Photochem. Photobiol.* **2014**, *90*, 667–672. [[CrossRef](#)]
10. Mandel, L. Hyposalivation: The Roles of Radioactive Iodine and Stapes Surgery. *J. Oral. Maxillofac. Surg.* **2013**, *71*, e76–e80. [[CrossRef](#)]
11. Ford, H.; Johnson, L.; Purdie, G.; Feek, C. Effects of Hyperthyroidism and Radioactive Iodine given to Ablate the Thyroid on the Composition of Whole Stimulated Saliva. *Clin. Endocrinol.* **1997**, *46*, 189–193. [[CrossRef](#)]
12. Almeida, J.P.; Kowalski, L.P. Pilocarpine Used to Treat Xerostomia in Patients Submitted to Radioactive Iodine Therapy: A Pilot Study Abstract. *Braz. J. Otorhinolaryngol.* **2010**, *76*, 659–662. [[CrossRef](#)]
13. Sunavala-Dossabhoy, G. Radioactive Iodine: An Unappreciated Threat to Salivary Gland Function. *Oral. Dis.* **2018**, *24*, 198–201. [[CrossRef](#)] [[PubMed](#)]
14. Tanasiewicz, M.; Hildebrandt, T.; Obersztyn, I. Xerostomia of Various Etiologies: A Review of the Literature. *Adv. Clin. Exp. Med.* **2016**, *25*, 199–206. [[CrossRef](#)] [[PubMed](#)]
15. Simões, A.; de Campos, L.; Arana-Chavez, V.E.; Nicolau, J. Low-Level Laser Therapy for Hyposalivation and Xerostomia. In *Lasers in Dentistry: Guide for Clinical Practice*; Freitas, P.M., Simões, A., Eds.; Wiley Blackwell: New York, NY, USA, 2015; Volume 1, pp. 335–339.
16. Saleh, J.; Figueiredo, M.A.Z.; Cherubini, K.; Braga-Filho, A.; Salum, F.G. Effect of Low-Level Laser Therapy on Radiotherapy-Induced Hyposalivation and Xerostomia: A Pilot Study. *Photomed. Laser Surg.* **2014**, *32*, 546–552. [[CrossRef](#)] [[PubMed](#)]
17. Pavlič, V. The Effects of Low-Level Laser Therapy on Xerostomia (Mouth Dryness). *Med. Pregl.* **2012**, *65*, 247–250. [[CrossRef](#)] [[PubMed](#)]
18. Lončar, B.; Stipetić, M.M.; Baričević, M.; Risović, D. The Effect of Low-Level Laser Therapy on Salivary Glands in Patients with Xerostomia. *Photomed. Laser Surg.* **2011**, *29*, 171–175. [[CrossRef](#)] [[PubMed](#)]
19. Golež, A.; Frangež, I.; Cankar, K.; Frangež, H.B.; Ovsenik, M.; Nemeth, L. Effects of Low-Level Light Therapy on Xerostomia Related to Hyposalivation: A Systematic Review and Meta-Analysis of Clinical Trials. *Lasers Med. Sci.* **2022**, *37*, 745–758. [[CrossRef](#)]
20. Lowry, O.H.; Rosebrough, N.J.; Farr, A.L.; Randall, R.J. Protein Measurement with the Folin Phenol Reagent. *J. Biol. Chem.* **1951**, *1*, 265–275. [[CrossRef](#)]
21. Chandra, A.; Dubey, A. Effect of Ploidy Levels on the Activities of  $\Delta$ 1-Pyrroline-5-Carboxylate Synthetase, Superoxide Dismutase and Peroxidase in Cenchrus Species Grown under Water Stress. *Plant Physiol. Biochem.* **2010**, *48*, 27–34. [[CrossRef](#)]
22. Anderson, L.C. Peroxidase release from rat submandibular salivary acinar cells in vitro. *Arch. Oral. Biol.* **1986**, *31*, 501–503. [[CrossRef](#)] [[PubMed](#)]
23. Aebi, H. Catalase in Vitro. *Methods Enzym.* **1984**, *105*, 121–126. [[CrossRef](#)]
24. Mor, G.; Alvero, A.B. Apoptosis and Cancer: Methods and Protocols: Second Edition. *Methods Mol. Biol.* **2014**, 1219. [[CrossRef](#)]
25. Choi, J.S.; Park, I.S.; Kim, S.K.; Lim, J.Y.; Kim, Y.M. Morphometric and Functional Changes of Salivary Gland Dysfunction after Radioactive Iodine Ablation in a Murine Model. *Thyroid* **2013**, *23*, 1445–1451. [[CrossRef](#)]
26. Spitzweg, C.; Joba, W.; Schriever, K.; Goellner, J.R.; Morris, J.C.; Heufelder, A.E. Analysis of Human Sodium Iodide Symporter Immunoreactivity in Human Exocrine Glands. *J. Clin. Endocrinol. Metab.* **1999**, *84*, 4178–4184. [[CrossRef](#)] [[PubMed](#)]
27. Nygaard, B.; Søres-Petersen, U.; Høilund-Carlsen, P.F.; Veje, A.; Holst, P.E.; Vestergaard, A.; Sølling, K. Improvement of Upper Airway Obstruction after 131 I-Treatment of Multinodular Nontoxic Goiter Evaluated by Flow Volume Loop Curves. *J. Endocrinol. Invest.* **1996**, *19*, 71–75. [[CrossRef](#)]

28. Walter, M.A.; Turtschi, C.P.; Schindler, C.; Minnig, P.; Müller-Brand, J.; Müller, B. The Dental Safety Profile of High-Dose Radioiodine Therapy for Thyroid Cancer: Long-Term Results of a Longitudinal Cohort Study. *J. Nucl. Med.* **2007**, *48*, 1620–1625. [[CrossRef](#)]
29. Jensen, S.B.; Pedersen, A.M.L.; Vissink, A.; Andersen, E.; Brown, C.G.; Davies, A.N.; Dutilh, J.; Fulton, J.S.; Jankovic, L.; Lopes, N.N.F.; et al. A Systematic Review of Salivary Gland Hypofunction and Xerostomia Induced by Cancer Therapies: Prevalence, Severity and Impact on Quality of Life. *Support Care Cancer* **2010**, *18*, 1039–1060. [[CrossRef](#)]
30. Erem, C.; Kandemir, N.; Hacıhasanoğlu, A.; Ersöz, H.Ö.; Ukcinc, K.; Kocak, M. Radioiodine Treatment of Hyperthyroidism Prognostic Factors Affecting Outcome. *Endocrine* **2004**, *25*, 55–60. [[CrossRef](#)]
31. Aktoz, T.; Durmus-Altun, G.; Usta, U.; Torun, N.; Ergulen, A.; Atakan, I.H. Radioiodine-Induced Kidney Damage and Protective Effect of Amifostine: An Experimental Study. *Hippokratia* **2012**, *16*, 40–45.
32. Bjordal, J.M.; Johnson, M.I.; Iversen, V.; Aimbire, F.; Lopes-Martins, R.A.B. Photoradiation in Acute Pain: A Systematic Review of Possible Mechanisms of Action and Clinical Effects in Randomized Placebo-Controlled Trials. *Photomed. Laser Surg.* **2006**, *24*, 158–168. [[CrossRef](#)]
33. Astuti, S.D.; Sulistyono, A.; Setiawatie, E.M.; Setiawatie, M.; Khasanah, M.; Purnobasuki, H.; Arifianto, D.; Susilo, Y.; Alamsyah, K.A.; Alamsyah, A. An In-Vivo Study of Photobiomodulation Using 403 Nm and 649 Nm Diode Lasers for Molar Tooth Extraction Wound Healing in Wistar Rats. *Odontology* **2022**, *110*, 240–253. [[CrossRef](#)]
34. Santos, N.R.S.; João, J.B.; Almeida, P.F.; Ribeiro, A.A.; Cangussú, M.C.T.; Dos Santos, J.N.; Pinheiro, A.L.B. Influence of the Combination of Infrared and Red Laser Light on the Healing of Cutaneous Wounds Infected by Staphylococcus Aureus. *Photomed. Laser Surg.* **2011**, *29*, 177–182. [[CrossRef](#)]
35. Nabaa, B.; Takahashi, K.; Sasaki, T.; Okizaki, A.; Aburano, T. Assessment of Salivary Gland Dysfunction after Radioiodine Therapy for Thyroid Carcinoma Using Non-Contrast-Enhanced CT: The Significance of Changes in Volume and Attenuation of the Glands. *Am. J. Neuroradiol.* **2012**, *33*, 1964–1970. [[CrossRef](#)]
36. La Perle, K.M.D.; Kim, D.C.; Hall, N.C.; Bobbey, A.; Shen, D.H.; Nagy, R.S.; Wakely, P.E.; Lehman, A.; Jarjoura, D.; Jhiang, S.M. Modulation of Sodium/Iodide Symporter Expression in the Salivary Gland. *Thyroid* **2013**, *23*, 1029–1036. [[CrossRef](#)]
37. Bourgeois, M.; Rajerison, H.; Guerard, F.; Mouglin-Degraef, M.; Barbet, J.; Michel, N.; Cherel, M.; Faivre-Chauvet, A.; Gustin, J.F. Iodine-131 for Therapy of Thyroid Diseases. *Nucl. Med. Rev.* **2011**, *14*, 90–95. [[CrossRef](#)]
38. Vanderpump, M.P.; Ahlquist, J.A.; Franklyn, J.A.; Clayton, R.N. Consensus Statement for Good Practice and Audit Measures in the Management of Hypothyroidism and Hyperthyroidism. *BMJ* **1996**, *31*, 539–544. [[CrossRef](#)]
39. Aydoğan, F.; Atilgan, H.I.; Koca, G.; Yumuşak, N.; Aydın, E.; Sadıç, M.; Korkmaz, M.; Tuncal, S.; Samim, E.E. An Evaluation of the Radioprotective Effect of Vitamin E on the Salivary Glands of Radioactive Iodine in Rats. *Kulak Burun Bogaz Ihtis. Derg* **2014**, *24*, 21–29. [[CrossRef](#)]
40. Mercadante, V.; Al Hamad, A.; Lodi, G.; Porter, S.; Fedele, S. Interventions for the Management of Radiotherapy-Induced Xerostomia and Hyposalivation: A Systematic Review and Meta-Analysis. *Oral. Oncol.* **2017**, *66*, 64–74. [[CrossRef](#)]
41. Saylam, G.; Baylır, Ö.; Gültekin, S.S.; Plnarlı, F.A.; Han, Ü.; Korkmaz, M.H.; Sancaktar, M.E.; Tatar, Y.; Sargon, M.F.; Tatar, E.C. Protective/Restorative Role of the Adipose Tissue-Derived Mesenchymal Stem Cells on the Radioiodine-Induced Salivary Gland Damage in Rats. *Radiol. Oncol.* **2017**, *51*, 307–318. [[CrossRef](#)]
42. Cheng, P.; Hollingsworth, B.; Scarberry, D.; Shen, D.H.; Powell, K.; Smart, S.C.; Beech, J.; Sheng, X.; Kirschner, L.S.; Menq, C.H.; et al. Automated MicroSPECT/MicroCT Image Analysis of the Mouse Thyroid Gland. *Thyroid* **2017**, *27*, 1433–1440. [[CrossRef](#)]
43. Elterman, K.G.; Mallampati, S.R.; Kaye, A.D.; Urman, R.D. Postoperative Alterations in Taste and Smell. *Anesthesiol. Pain. Med.* **2014**, *4*, e18527. [[CrossRef](#)]

**Disclaimer/Publisher’s Note:** The statements, opinions and data contained in all publications are solely those of the individual author(s) and contributor(s) and not of MDPI and/or the editor(s). MDPI and/or the editor(s) disclaim responsibility for any injury to people or property resulting from any ideas, methods, instructions or products referred to in the content.